Wavelet correlations in the p model

Martin Greiner*
Department of Physics, University of Arizona, Tucson, Arizona 85721
and Institut für Theoretische Physik, Justus Liebig Universität, 35392 Gießen, Germany

Peter Lipa† and Peter Carruthers‡
Department of Physics, University of Arizona, Tucson, Arizona 85721
(Received 3 December 1993; revised manuscript received 22 June 1994)

We suggest applying the concept of wavelet transforms to the study of correlations in multiparticle physics. Both the usual correlation functions as well as the wavelet transformed ones are calculated for the p model, which is a simple but tractable random cascade model. For this model, the wavelet transform decouples correlations between fluctuations defined on different scales. The advantageous properties of factorial moments are also shared by properly defined factorial wavelet correlations.

PACS number(s): 05.40.+j, 13.65.+i, 13.85.Hd, 47.27.−i

I. INTRODUCTION

The concepts of scaling and self-similar fluctuations gain increasing importance in the study of many different stochastic processes such as phase transitions, turbulence, galaxy clustering, and multiparticle production. The unifying feature of such diverse processes is an approximate power law behavior of the correlation functions. Unfortunately, correlation functions higher than second order are hard to measure directly; therefore appropriate averaging and/or transformation techniques have to be applied in order to extract information of interest.

In the context of multiparticle physics useful tools such as factorial moments, G moments, cumulants, correlation integrals, void probabilities, and combinants [1–3] are currently explored and to some extent already applied to the analysis of data. These correlation measures elucidate many interesting features of multiparticle correlations and are used, for example, to detect a possible fractal structure of QCD parton shower cascades [4]. Here we explore a new approach, namely, *wavelet transformed* correlation functions, or short, wavelet correlations.

The analysis of irregular textures by means of the wavelet transform has by now gained widespread application in many different fields, most notably in signal processing, data compression, and pattern recognition [5–8]. Its central property is the possibility to resolve an arbitrary function *simultaneously* in terms of its standard variable (say time) and its conjugate counterpart in Fourier space (in this case frequency) in an efficient manner. This is achieved by an expansion of the function with respect to a self-similar set of (not necessarily) orthogonal basis functions, so-called wavelets. These techniques have not yet been applied to the analysis of irregular and possibly fractal point processes arising in multiparticle production at high energies.

For the present study the self-similarity aspect of the wavelet basis is crucial. More specifically, the whole basis is constructed from dilations and translations (affine transformations) of one single "mother" wavelet. Such an affine basis may be understood as a "mathematical microscope," which is optimized to dissect structures on finer and finer scales. In other words, the wavelet transform separates "spikes" or "clusters" existing at very different scales in a signal.

Both the self-similarity aspect of the wavelet basis as well as the above mentioned "scale separation property" of the wavelet transform lead us to the suspicion that the latter might be a very convenient tool for the representation and analysis of cascade processes. The wavelet correlations of selfsimilar processes, to be more precise, the correlations between the coefficients of a wavelet expansion, will be "quasidiagonal," i.e., an appropriately chosen wavelet basis is a "natural" close approximation to the true eigenfunctions.

Such a quasidiagonalization of the covariance matrix has already been demonstrated for some self-similar stochastic processes such as fractional Brownian motion [9]. In the general case the true eigenfunctions are difficult (if not impossible) to find, so that one has to choose between various types of wavelet bases in order to find out which one will lead to an "optimal quasidiagonalization" [7].

The goals for this paper are modest. For a demonstration of wavelet techniques with respect to self-similar cascades we have chosen the one-dimensional p-model cascade [10], which has been developed to describe the energy dissipation in fully developed turbulence. Together with the closely related α model it has also been used as a

*Electronic address: TP21@DDAGSI3.GSI.DE
†Current address: Institut für Hochenergiephysik der Österreichischen Akademie der Wissenschaften, A-1050 Wien, Austria; electronic address: LIPA@HEPHY.OEAW.AC.AT
‡Electronic address: CARRUTHERS@CCIT.ARIZONA.EDU

simple discrete approximation to multiparticle processes in high energy e^+e^- and hadron-hadron collisions [1,11]. Here the p model serves as a tractable toy model to study wavelet correlations analytically. The p model is special also in another way: the simplest of all wavelets, the Haar wavelet, represents an exact set of eigenfunctions for the covariance matrix.

After a brief introduction to the wavelet concept in Sec. II, we first calculate the conventional correlation densities of the p model in Sec. III and then turn to the direct determination of the Haar-wavelet correlation densities. Furthermore, a general approach is developed to study correlations with respect to any orthogonal wavelet basis. Section IV is devoted to the study of the p model with Poissonian noise and to the application of the wavelet transform on factorial moment and cumulant densities, which are so crucial in the study of point processes. The conclusions are presented in Sec. V.

II. SOME BASICS OF WAVELETS

We will summarize only some very basic concepts of wavelets and the related idea of a *multiresolution analysis*. For a more profound introduction we refer the reader to some excellent reviews [5–8].

Given an arbitrary and, for simplicity, one-dimensional function $\epsilon(x)$ supported in the interval $[0,1]$, we seek to approximate it in terms of a histogram with 2^J bins. A histogram is a collection of individual bins represented by the set of box functions

$$\phi^H_{Jk}(x) = \phi^H(2^J x - k) = \begin{cases} 1 & \text{for } k2^{-J} \le x < (k+1)2^{-J} \\ 0 & \text{otherwise} , \end{cases} \tag{2.1}$$

which are all constructed from the unit box function $\phi^H_{00}(x)$ by a discrete dilation factor 2^J and a translation governed by an integer k. Within a given scale the box functions $\phi^H_{Jk}(x)$ are orthogonal with respect to the shift index k.

The approximation of the function $\epsilon(x)$ at the finest scale J is then written as a histogram:

$$\epsilon(x) \to \epsilon^{(J)}(x) = \sum_k \epsilon^{(J)}_k \phi^H_{Jk}(x) \ ; \tag{2.2}$$

compare with the upper left histogram of Figs. 1 and 2(a). If we were to approximate $\epsilon(x)$ with the box functions $\phi^H_{J-1,k}$ belonging to the rougher resolution scale $J-1$, which are again orthogonal with respect to the shift index k, but are not orthogonal to the box functions ϕ^H_{Jk} of the finer "resolution" scale J, evidently some detail is lost compared to the approximation (2.2). This detail is the difference between approximations (2.2) with resolution scales J and $J-1$. It can be fully expressed in terms of the difference functions $\psi^H_{J-1,k}(x) = \psi^H(2^{J-1}x - k)$ with

$$\psi^H_{00}(x) = \psi^H(x) = \begin{cases} 1 & \text{for } 0 \le x < 1/2 \\ -1 & \text{for } 1/2 \le x < 1 \\ 0 & \text{otherwise} . \end{cases} \tag{2.3}$$

Again the functions $\psi^H_{J-1,k}(x)$ are orthogonal with respect to the shift index k within the given resolution

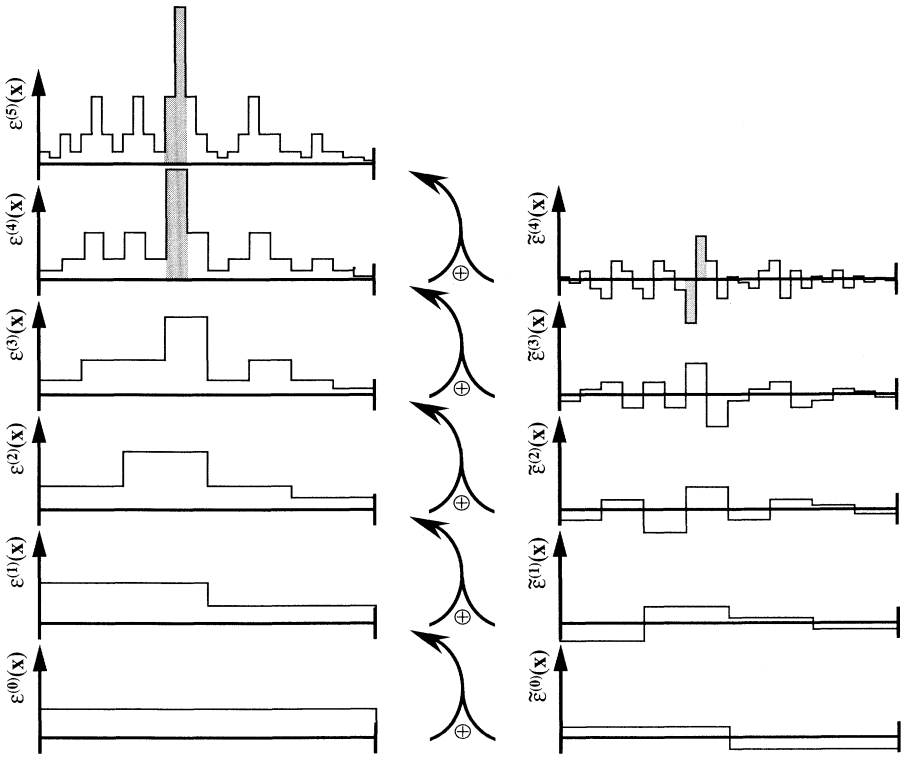

FIG. 1. Multiresolution decomposition of a random function (upper left corner) at initial resolution scale $J = 5$ with respect to the Haar-wavelet basis. The left column shows a sequence of approximations to the original signal, while the right column represents the Haar-wavelet transform of $\epsilon^{(5)}(x)$.

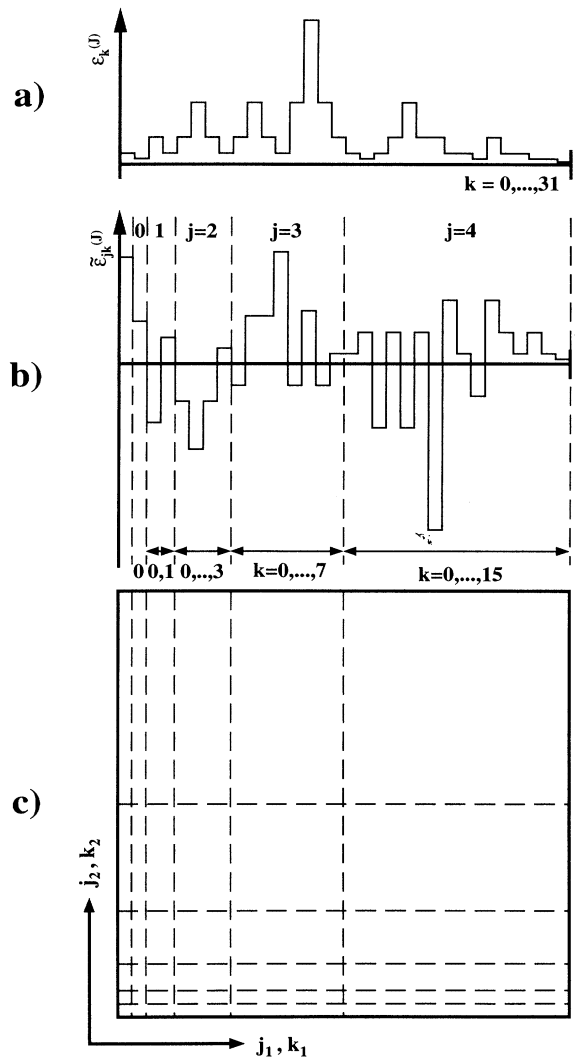

FIG. 2. Numbering scheme of (a) the original amplitudes $\epsilon_k^{(J)}$ and (b) of the Haar-wavelet transformed amplitudes $\tilde{\epsilon}_{jk}^{(J)}$. (c) shows the structure of the second-order correlation matrix of the wavelet amplitudes.

scale $J-1$; they are also orthogonal to the box functions $\phi_{J-1,k}^H(x)$ at scale $J-1$, but are not orthogonal to the box functions $\phi_{Jk}^H(x)$ at scale J. On the other hand, the $\phi_{Jk}^H(x)$ are expressible in terms of the $\phi_{J-1,k}^H(x)$ and $\psi_{J-1,k}^H(x)$, together; we get, for example,

$$\phi_{10}^H(x) = \frac{1}{2}[\phi_{00}^H(x) + \psi_{00}^H(x)],$$
$$\phi_{11}^H(x) = \frac{1}{2}[\phi_{00}^H(x) - \psi_{00}^H(x)] \ . \tag{2.4}$$

This defines a *multiresolution analysis* of the function $\epsilon(x)$: At first $\epsilon(x)$ is approximated with box functions $\phi_{Jk}^H(x)$ of scale J according to Eq. (2.2). Then according to Eq. (2.4) the $\phi_{Jk}^H(x)$ are expressed in terms of box functions $\phi_{J-1,k}^H(x)$ and the difference functions $\psi_{J-1,k}^H(x)$ both of lower scale $J-1$. Thereafter the $\phi_{J-1,k}^H(x)$ are rewritten in terms of $\phi_{J-2,k}^H(x)$ and $\psi_{J-2,k}^H(x)$ and so on. Going from one scale j to the next lower scale $j-1$, only the difference between the two resolutions is memorized and expressed in terms of the difference functions $\psi_{j-1,k}^H(x)$. This procedure is depicted in Fig. 1. As a consequence of this multiresolution analysis, the amplitudes $\epsilon_k^{(J)}$ of the box functions at the finest scale J are transformed into the amplitudes $\tilde{\epsilon}_{jk}^{(J)}$ of the difference functions with scales in the range $0 \le j \le J-1$ together with the amplitude $\epsilon_0^{(0)}$ of the box function at the roughest scale j=0:

$$\begin{aligned}\epsilon^{(J)}(x) &= \sum_k \epsilon_k^{(J)} \phi_{Jk}^H(x) \\ &= \epsilon^{(0)}(x) + \sum_{j=0}^{J-1} \tilde{\epsilon}^{(j)}(x) \\ &= \epsilon_0^{(0)} \phi_{00}^H(x) + \sum_{j=0}^{J-1} \sum_{k=0}^{2^j-1} \tilde{\epsilon}_{jk}^{(J)} \psi_{jk}^H(x) \ ;\end{aligned} \tag{2.5}$$

confer again Fig. 1.

The "difference" amplitudes

$$\tilde{\epsilon}_{jk} = 2^j \int \epsilon(x) \psi_{jk}^H(x) dx \tag{2.6}$$

are most conveniently represented in a one-dimensional histogram with 2^J bins

$$(\epsilon_0^{(0)}, \tilde{\epsilon}_{00}, \tilde{\epsilon}_{10}, \tilde{\epsilon}_{11}, \tilde{\epsilon}_{20}, \ldots, \tilde{\epsilon}_{23}, \tilde{\epsilon}_{30}, \ldots, \tilde{\epsilon}_{J-1,2^{J-1}-1}), \tag{2.7}$$

as depicted in Fig. 2(b).

In general the difference function $\psi_{jk}(x)$ is called a wavelet and the approximation function $\phi_{jk}(x)$ the corresponding scaling function. More formally they are defined via the dilation equations

$$\phi(x) = \sum_m c_m \, \phi(2x - m) \tag{2.8}$$

and

$$\psi(x) = \sum_m (-1)^m c_{1-m} \, \phi(2x - m) \ , \tag{2.9}$$

where the finite number of nonzero coefficients c_m have to satisfy various conditions stated by Daubechies [6]. Once a finite set of admissible c_m is chosen, the solutions ϕ and ψ can be found by (numerical) iteration of Eqs. (2.8) and (2.9).

The scaling function $\phi^H(x)$ of Eq. (2.1) and the Haar wavelet $\psi^H(x)$ of Eq. (2.3) represent the simplest example; for them the only nonvanishing coefficients are $c_0 = c_1 = 1$. However, the Haar wavelet has a serious drawback: It is discontinuous and, consequently, not very well localized in Fourier space. Better localization properties in Fourier space are given, for example, with the choices

$$\begin{aligned} c_0 &= \tfrac{1}{4}(1+\sqrt{3}) \ , & c_1 &= \tfrac{1}{4}(3+\sqrt{3}) \ , \\ c_2 &= \tfrac{1}{4}(3-\sqrt{3}) \ , & c_3 &= \tfrac{1}{4}(1-\sqrt{3}) \ , \end{aligned} \tag{2.10}$$

leading to the smoother orthogonal Daubechies D4

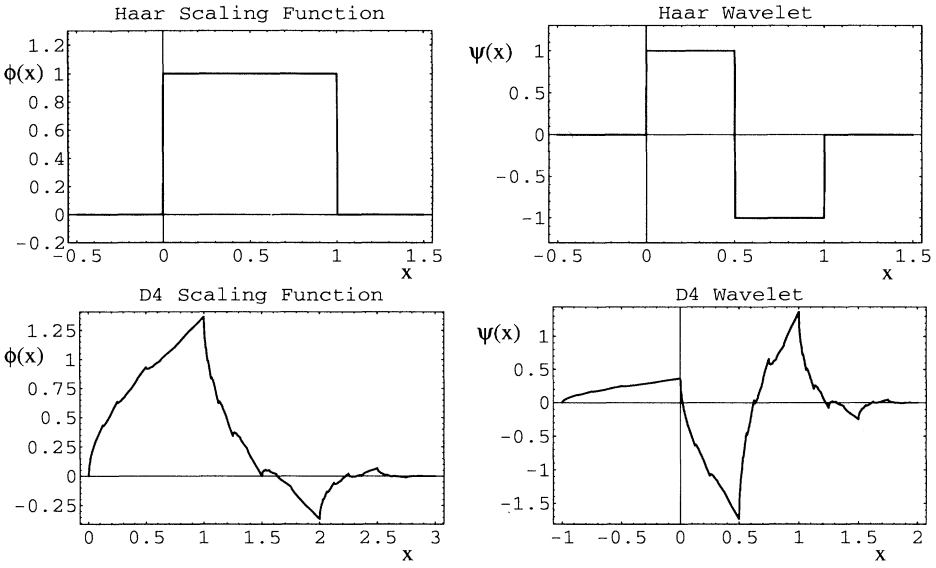

FIG. 3. Scaling function and wavelet for the Haar and Daubechies D4 cases, respectively.

wavelet [6]. These wavelets and their corresponding scaling functions are exemplified in Fig. 3. Note that the D4 wavelet is still compact, but three times as wide as the Haar wavelet.

Both examples shown reflect a compact support. In the literature many different wavelets with various additional properties have been constructed and used. Generally one has a trade-off between compactness and smoothness of a wavelet: the smoother the wavelet becomes (and thus the better it is localized in Fourier space), the broader the compact support has to be.

As a generalization of the multiresolution analysis presented for the Haar wavelet before, Eqs. (2.5), (2.8), and (2.9) define a multiresolution analysis for any specific choice of wavelets. The resulting "histograms" at the various scales then acquire the smoothness of the underlying scaling function and wavelet.

III. p MODEL AND CORRELATION DENSITIES

We will briefly introduce the p model, which successfully describes the multifractal spectrum of the energy dissipation in turbulent flow [10]. We determine its conventional correlation densities as well as its Haar-wavelet correlation densities analytically. Because of its more complicated structure, we finally exhibit the results of a computerized calculation for the Daubechies D4-wavelet correlation densities.

A. p model

Without any loss of generality we consider the interval [0,1] and normalize the "energy" E to unity in this interval. We then split this interval into two equal parts with energies $E_1 = pE$ and $E_2 = (1-p)E$, where E_1 goes randomly, with equal probability, to the left or right subinterval (bin). Let us pick the left subinterval and say it goes with the energy E_1; we then split this subinterval again into two parts with corresponding energies $E_1' = pE_1$ and $E_2' = (1-p)E_1$, where again E_1' goes randomly to the new left or right subinterval. For the right subinterval we proceed in the same way. The whole procedure is repeated over and over again; see Fig. 4. For

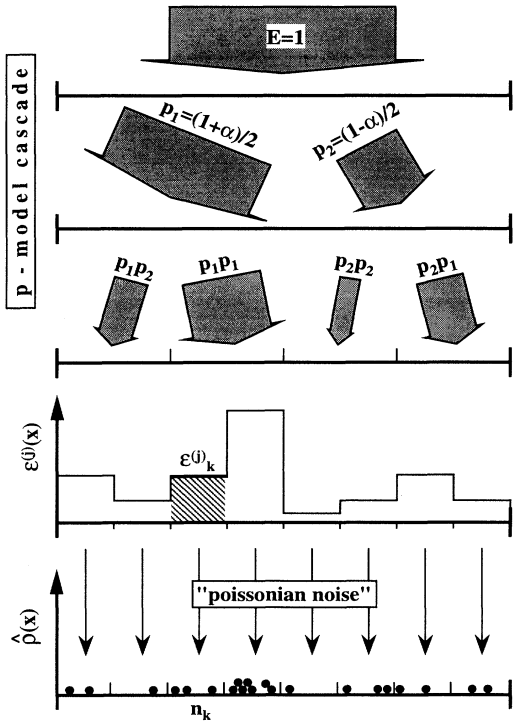

FIG. 4. p-model cascade, where towards smaller scales the length of the interval is divided into two halves and the flux of energy is transferred in nonequal fractions $p_1 = (1+\alpha)/2$ and $p_2 = (1-\alpha)/2$. At the last step a particle number is tossed in each bin according to a Poisson distribution with mean $\bar{n}\epsilon_k^{(J)}$.

later convenience we set the "splitting" parameter equal to

$$p = p_1 = \frac{1}{2}(1+\alpha), \quad (1-p) = p_2 = \frac{1}{2}(1-\alpha) \tag{3.1}$$

with $0 \leq \alpha \leq 1$. Clearly the total energy is conserved in this cascade. The energy density contained in a certain subinterval is defined as the corresponding energy divided by the length of the subinterval; let us denote the energy density as $\epsilon_k^{(J)}$, where the index J ($J \geq 0$) represents the actual scale (equal to the number of cascade steps) and the index k ($0 \leq k \leq 2^J - 1$) represents the kth subinterval belonging to the scale J. Also as the scale parameter J increases, the number of possible configurations increases with $2^{(2^J-1)}$. Within a given scale each configuration μ occurs with the same probability, i.e., $p_\mu^{(J)} = 2^{-(2^J-1)}$.

B. Bin correlation densities

The one-bin correlation density is defined as the configuration average $\langle\,\rangle$ of the energy density in the bin k_1 at some scale j:

$$\rho_{k_1}^{(j)} = \sum_\mu p_\mu^{(j)} \epsilon_{k_1^{(\mu)}}^{(j)} = \langle \epsilon_{k_1}^{(j)} \rangle \,. \tag{3.2}$$

In an analogous manner, the two-, three-, etc. bin correlation densities are given by

$$\begin{aligned} \rho_{k_1,k_2}^{(j)} &= \langle \epsilon_{k_1}^{(j)} \epsilon_{k_2}^{(j)} \rangle \quad , \\ \rho_{k_1,k_2,k_3}^{(j)} &= \langle \epsilon_{k_1}^{(j)} \epsilon_{k_2}^{(j)} \epsilon_{k_3}^{(j)} \rangle \ , \ldots \quad . \end{aligned} \tag{3.3}$$

For convenience we consider the characteristic function for the correlation densities:

$$\begin{aligned} Z^{(j)}[\vec{\lambda}^{(j)}] &= \left\langle \exp\left(i \sum_{k=0}^{2^j-1} \lambda_k^{(j)} \epsilon_k^{(j)} \right) \right\rangle \\ &= 1 + i \sum_{k_1} \lambda_{k_1}^{(j)} \rho_{k_1}^{(j)} + \frac{i^2}{2!} \sum_{k_1,k_2} \lambda_{k_1}^{(j)} \lambda_{k_2}^{(j)} \rho_{k_1,k_2}^{(j)} \\ &\quad + \frac{i^3}{3!} \sum_{k_1,k_2,k_3} \lambda_{k_1}^{(j)} \lambda_{k_2}^{(j)} \lambda_{k_3}^{(j)} \rho_{k_1,k_2,k_3}^{(j)} + \cdots \,, \end{aligned} \tag{3.4}$$

where we use an abbreviated notation $\vec{\lambda}^{(j)}$ for the collection of parameters $(\lambda_0, \ldots, \lambda_{2^j-1})$. Once the characteristic function is known analytically, the correlation densities between $2, 3, \ldots, q$ bins (or the qth cumulant) can be obtained by partial derivatives of qth order of $Z[\vec{\lambda}]$ (or $\ln Z[\vec{\lambda}]$) with respect to $\lambda_k^{(j)}$:

$$\rho_{k_1,\ldots,k_q}^{(j)} = \frac{1}{i^q} \frac{\partial^q Z^{(j)}[\vec{\lambda}^{(j)}]}{\partial \lambda_{k_1}^{(j)} \cdots \partial \lambda_{k_q}^{(j)}} \bigg|_{\vec{\lambda}^{(j)}=0} \,. \tag{3.5}$$

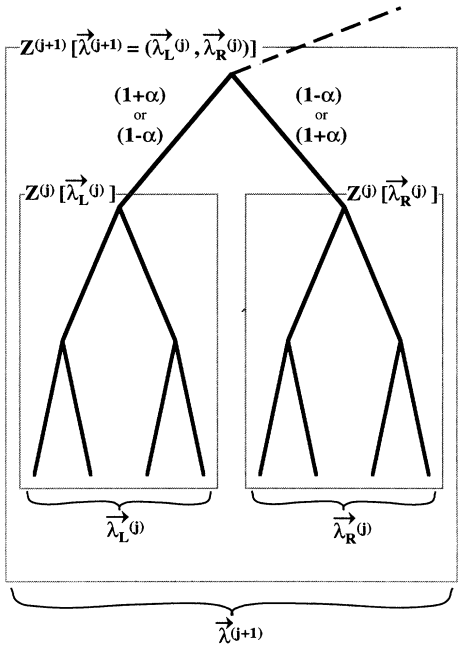

FIG. 5. Recursive construction of the characteristic function for the p model.

We introduce an iterative scheme for the characteristic function, which allows us to calculate it at one scale recursively from the next rougher scale. Figure 5 represents a diagram of how the possible p-model configurations at scale $j+1$ evolve from configurations at scale j. Let us say that we know all the possible configurations for the energy densities in the 2^j bins at a given scale j. The dyadic tree at scale $j+1$ is then composed of a left and a right sub-tree, each at scale j. The branching to the left might be weighted with the splitting factor $(1+\alpha)$, so that the branching to the right has to go with $(1-\alpha)$ or vice versa.

We use the explicit form of the characteristic function (3.4) at scale $j+1$; in the spirit of Fig. 5 we split the 2^{j+1} variables collected in $\vec{\lambda}^{(j+1)} = (\vec{\lambda}_L^{(j)}, \vec{\lambda}_R^{(j)})$ into a left (L) and a right (R) subset. It follows that

$$\begin{aligned} Z^{(j+1)}[\vec{\lambda}^{(j+1)}] &= \sum_\mu p_\mu^{(j+1)} \exp\left(i \sum_{k=0}^{2^{j+1}-1} \lambda_k^{(j+1)} \epsilon_{k^{(\mu)}}^{(j+1)} \right) \\ &= \sum_{\mu^+} p_{\mu^+}^{(j+1)} \exp\left(i \sum_{k_L=0}^{2^j-1} (1+\alpha) \lambda_{k_L}^{(j)} \epsilon_{k_L^{(\mu^+)}}^{(j)} \right) \exp\left(i \sum_{k_R=0}^{2^j-1} (1-\alpha) \lambda_{k_R}^{(j)} \epsilon_{k_R^{(\mu^+)}}^{(j)} \right) \\ &\quad + \sum_{\mu^-} p_{\mu^-}^{(j+1)} \exp\left(i \sum_{k_L=0}^{2^j-1} (1-\alpha) \lambda_{k_L}^{(j)} \epsilon_{k_L^{(\mu^-)}}^{(j)} \right) \exp\left(i \sum_{k_R=0}^{2^j-1} (1+\alpha) \lambda_{k_R}^{(j)} \epsilon_{k_R^{(\mu^-)}}^{(j)} \right) \,. \end{aligned} \tag{3.6}$$

If the branching of the dyadic tree at scale $j+1$ to the left goes with $(1+\alpha)$ and to the right with $(1-\alpha)$, the configurations μ^+ at scale $j+1$ are defined; for the μ^- configurations it is the other way round. Observe that the configuration probability at scale $j+1$

$$p_\mu^{(j+1)} = 2^{-(2^{j+1}-1)} = \frac{1}{2}\left(2^{-(2^j-1)}\right)^2 = \frac{1}{2}\left(p_\mu^{(j)}\right)^2 \tag{3.7}$$

factorizes into the product of the configuration probabilities at scale j. This allows us to write the sum $\sum_\mu$ over all scale $j+1$ configurations as a double sum $\sum_{\mu_L}\sum_{\mu_R}$ over all scale j left and right configurations. We then obtain the recursion relation for the characteristic function of the p model:

$$Z^{(j+1)}[\vec{\lambda}^{(j+1)}] = \frac{1}{2}\{Z^{(j)}[(1+\alpha)\vec{\lambda}_L^{(j)}]\, Z^{(j)}[(1-\alpha)\vec{\lambda}_R^{(j)}] + Z^{(j)}[(1-\alpha)\vec{\lambda}_L^{(j)}]\, Z^{(j)}[(1+\alpha)\vec{\lambda}_R^{(j)}]\}\ , \tag{3.8}$$

with $Z^{(0)}[\lambda^{(0)}] = \exp(i\lambda^{(0)})$.

This iterative solution for the characteristic function can now be used to derive recursion relations for the correlation densities (3.5). First, as an explicit demonstration of this, the two-bin correlation density $\rho_{k_1,k_2}^{(j+1)}$ is considered for the special case that both $\lambda_{k_1}^{(j+1)}$ and $\lambda_{k_2}^{(j+1)}$ belong to $\vec{\lambda}_L^{(j)}$, i.e., to the left branch of the dyadic tree depicted in Fig. 5; we get

$$\begin{aligned}\rho_{k_1,k_2}^{(j+1)} &= \frac{1}{2i^2}\left(\frac{\partial^2 Z^{(j)}[\vec{\lambda}_L^{(j)}]}{\partial\lambda_{k_1}^{(j)}\partial\lambda_{k_2}^{(j)}}(1+\alpha)^2 Z^{(j)}[(1-\alpha)\vec{\lambda}_R^{(j)}] + \frac{\partial^2 Z^{(j)}[\vec{\lambda}_L^{(j)}]}{\partial\lambda_{k_1}^{(j)}\partial\lambda_{k_2}^{(j)}}(1-\alpha)^2 Z^{(j)}[(1+\alpha)\vec{\lambda}_R^{(j)}]\right)\Bigg|_{\vec{\lambda}^{(j+1)}=0} \\ &= (1+\alpha^2)\rho_{k_1,k_2}^{(j)}\ ,\end{aligned}$$

where $Z^{(j)}[\vec{\lambda}^{(j)}]|_{\vec{\lambda}=0} = 1$ and Eq. (3.5) have been used. In general we find, for the correlation densities,

$$\rho_{k_1}^{(j)} = 1 \quad , \tag{3.9}$$

$$\rho_{k_1,k_2}^{(j+1)} = \begin{cases} (1+\alpha^2)\rho_{k_1,k_2}^{(j)} & \text{if } k_1,k_2 \in \{L\} \\ (1+\alpha^2)\rho_{k_1-2^j,k_2-2^j}^{(j)} & \text{if } k_1,k_2 \in \{R\} \\ (1-\alpha^2) & \text{if } k_1 \in \{L\} \text{ and } k_2 \in \{R\} \text{ or vice versa,} \end{cases} \tag{3.10}$$

$$\rho_{k_1,k_2,k_3}^{(j+1)} = \begin{cases} (1+3\alpha^2)\rho_{k_1,k_2,k_3}^{(j)} & \text{if } k_1,k_2,k_3 \in \{L\},\dots, \\ (1-\alpha^2)\rho_{k_1,k_2}^{(j)} & \text{if } k_1,k_2 \in \{L\} \text{ and } k_3 \in \{R\},\dots. \end{cases} \tag{3.11}$$

$\{L\}$ and $\{R\}$ stand for all the bins belonging to the left and the right branch of the dyadic tree depicted in Fig. 5. For the right branch the indices have to be shifted as indicated above for the two-bin correlation density only.

The one-bin density is equal to one as it should be, because energy is conserved in the p model, so that the average energy density on every scale j is equal to the initial density. The two-bin correlation density is depicted in Fig. 6; it shows clearly the multiplicative structure (3.10) as the scale becomes finer. The closer the bins are together, the stronger they are correlated; a scaling law with decreasing bin-bin distance shows up as a result of the self-similarity of the p-model cascade.

It is straightforward to rewrite the recursion relations (3.9)–(3.11) of the correlation densities in terms of cumulant densities, the latter having the advantage that they subtract contributions from lower-order correlations. We find

$$C_{k_1}^{(j)} = \rho_{k_1}^{(j)} = 1, \tag{3.12}$$

$$\begin{aligned} C_{k_1,k_2}^{(j+1)} &= \rho_{k_1,k_2}^{(j+1)} - \rho_{k_1}^{(j+1)}\rho_{k_2}^{(j+1)} \\ &= \begin{cases} (1+\alpha^2)C_{k_1,k_2}^{(j)} + \alpha^2 & \text{if } k_1,k_2 \in \{L\},\dots \\ -\alpha^2 & \text{if } k_1 \in \{L\} \text{ and } k_2 \in \{R\} \text{ or vice versa,} \end{cases} \end{aligned} \tag{3.13}$$

$$\begin{aligned} C_{k_1,k_2,k_3}^{(j+1)} &= \rho_{k_1,k_2,k_3}^{(j+1)} - \rho_{k_1,k_2}^{(j+1)}\rho_{k_3}^{(j+1)} - \rho_{k_1,k_3}^{(j+1)}\rho_{k_2}^{(j+1)} - \rho_{k_2,k_3}^{(j+1)}\rho_{k_1}^{(j+1)} + 2\rho_{k_1}^{(j+1)}\rho_{k_2}^{(j+1)}\rho_{k_3}^{(j+1)} \\ &= \begin{cases} (1+3\alpha^2)C_{k_1,k_2,k_3}^{(j)} + 2\alpha^2(C_{k_1,k_2}^{(j)} + C_{k_1,k_3}^{(j)} + C_{k_2,k_3}^{(j)}) & \text{if } k_1,k_2,k_3 \in \{L\},\dots \\ -2\alpha^2 C_{k_1,k_2}^{(j)} & \text{if } k_1,k_2 \in \{L\} \text{ and } k_3 \in \{R\},\dots. \end{cases} \end{aligned} \tag{3.14}$$

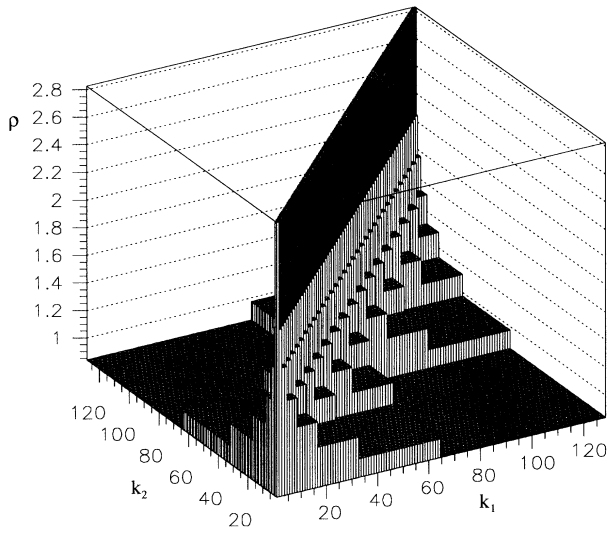

FIG. 6. Two-bin correlation density $\rho_{k_1 k_2}$ after $J = 7$ p-model cascade steps ($\alpha = 0.4$).

Evidently, the cumulant densities show a recursive structure that is analogous to the correlation densities (3.9)–(3.11).

C. Haar-wavelet correlation densities

So far we have determined the correlation (and cumulant) densities between the various bins at the last step of the p-model cascade. If we would first average over several adjacent bins and then study the correlations of the local averages, we could extract information about earlier stages of the cascade; referring to the left column in Fig. 1, this would correspond to the analysis of correlations among the amplitudes within each averaged histogram $\epsilon^{(j)}(x)$ separately. Obviously this procedure yields highly redundant information since the correlations at a given scale also include the correlations at all rougher scales.

As an alternative we suggest studying correlations between *differences of bin amplitudes at adjacent scales*; in other words, we look at correlations among the difference amplitudes of the right column histograms $\tilde{\epsilon}^{(j)}(x)$ of Fig. 1. Since each such histogram reflects the difference of fluctuations at two adjacent scales only and thus is independent of the fluctuations at earlier stages (scales) of the cascade, this approach contains no redundancy at all. At this point the wavelets enter the picture.

For an elementary outline we consider the Haar wavelet first. In this case the wavelet decomposition (2.5) gives us the amplitude

$$\epsilon_0^{(0)} = \frac{1}{2^J} \sum_{k=0}^{2^J-1} \epsilon_k = 1 \quad , \tag{3.15}$$

representing the mean energy density, and the Haar-wavelet amplitudes

$$\begin{aligned}
\tilde{\epsilon}_{00} &= \frac{1}{2^J} \left(\sum_{k=0}^{2^{J-1}-1} \epsilon_k - \sum_{k=2^{J-1}}^{2^J-1} \epsilon_k \right) , \\
\tilde{\epsilon}_{10} &= \frac{1}{2^{J-1}} \left(\sum_{k=0}^{2^{J-2}-1} \epsilon_k - \sum_{k=2^{J-2}}^{2^{J-1}-1} \epsilon_k \right) , \\
\tilde{\epsilon}_{11} &= \frac{1}{2^{J-1}} \left(\sum_{k=2^{J-1}}^{3\cdot 2^{J-2}-1} \epsilon_k - \sum_{k=3\cdot 2^{J-2}}^{2^J-1} \epsilon_k \right) , \\
\tilde{\epsilon}_{20} &= \frac{1}{2^{J-2}} \left(\sum_{k=0}^{2^{J-3}-1} \epsilon_k - \sum_{k=2^{J-3}}^{2^{J-2}-1} \epsilon_k \right) , \qquad (3.16) \\
&\vdots \\
\tilde{\epsilon}_{J-1,0} &= \frac{1}{2} \left(\epsilon_0 - \epsilon_1 \right) , \\
\tilde{\epsilon}_{J-1,1} &= \frac{1}{2} \left(\epsilon_2 - \epsilon_3 \right) , \ \ldots \ , \\
\tilde{\epsilon}_{J-1,2^{J-1}-1} &= \frac{1}{2} \left(\epsilon_{2^J-2} - \epsilon_{2^J-1} \right) ,
\end{aligned}$$

representing the difference between partial mean energy densities, where "partial" depends on the position within the dyadic cascade. We want to stress one more time that, according to Eq. (2.5), both the energy density histogram at scale J as well as the Haar-wavelet amplitudes completely represent the specific configuration μ at scale J. Note also that we have suppressed the configuration index μ for the wavelet amplitudes in Eqs. (3.15) and (3.16).

Analogously to Eqs. (3.2) and (3.3), the correlations between the various Haar-wavelet coefficients of Eqs. (3.15) and (3.16) are defined by

$$\begin{aligned}
\tilde{\rho}_{(j_1 k_1)} &= \langle \tilde{\epsilon}_{j_1 k_1} \rangle \ , \\
\tilde{\rho}_{(j_1 k_1),(j_2 k_2)} &= \langle \tilde{\epsilon}_{j_1 k_1} \tilde{\epsilon}_{j_2 k_2} \rangle \ , \qquad (3.17) \\
\tilde{\rho}_{(j_1 k_1),(j_2 k_2),(j_3 k_3)} &= \langle \tilde{\epsilon}_{j_1 k_1} \tilde{\epsilon}_{j_2 k_2} \tilde{\epsilon}_{j_3 k_3} \rangle \ .
\end{aligned}$$

In order to extract the Haar-wavelet correlations of the p model analytically, we express the bin energy densities ϵ_k, entering the exponent of the characteristic function (3.4), in terms of the wavelet amplitudes $\tilde{\epsilon}_{jk}$; as a consequence, we introduce variation parameters η_{jk}, so that

$$\sum_{k=0}^{2^J-1} \lambda_k \epsilon_k = \sum_{j=0}^{J-1} \sum_{k=0}^{2^j-1} \eta_{jk} \tilde{\epsilon}_{jk} + \eta_0 \epsilon_0^{(0)} \ . \tag{3.18}$$

Apart from factors 2^{-j}, these η_{jk} can be understood as the wavelet transform of the λ_k:

$$\eta_0 = \sum_{k=0}^{2^J-1} \lambda_k \quad ,$$
$$\eta_{00} = \sum_{k=0}^{2^{J-1}-1} \lambda_k - \sum_{k=2^{J-1}}^{2^J-1} \lambda_k \quad ,$$
$$\eta_{10} = \sum_{k=0}^{2^{J-2}-1} \lambda_k - \sum_{k=2^{J-2}}^{2^{J-1}-1} \lambda_k \quad ,$$
$$\eta_{11} = \sum_{k=2^{J-1}}^{3\cdot 2^{J-2}-1} \lambda_k - \sum_{k=3\times 2^{J-2}}^{2^J-1} \lambda_k \quad ,$$
$$\vdots \tag{3.19}$$
$$\eta_{J-1,0} = \lambda_0 - \lambda_1 \ ,$$
$$\eta_{J-1,1} = \lambda_2 - \lambda_3 \ , \ \ldots \ , \ \eta_{J-1,2^{J-1}-1} = \lambda_{2^J-2} - \lambda_{2^J-1} \ ;$$

compare with Eqs. (3.15) and (3.16).

Furthermore, we introduce a left-right branch splitting of the $\vec{\eta}$ variables

$$\eta_0^{(j+1)} = \sum_{k=0}^{2^j-1} \lambda_k^{(j+1)} + \sum_{k=2^j}^{2^{j+1}-1} \lambda_k^{(j+1)} = \eta_{0;L}^{(j)} + \eta_{0;R}^{(j)},$$
$$\eta_{00}^{(j+1)} = \eta_{0;L}^{(j)} - \eta_{0;R}^{(j)}, \tag{3.20}$$
$$\eta_{j'k'}^{(j+1)} = \begin{cases} \eta_{j'-1,k';L}^{(j)} & \text{for } k' = 0, \ldots, 2^{j'-1}-1 \\ \eta_{j'-1,k'-2^{j'-1};R}^{(j)} & \text{for } k' = 2^{j'-1}, \ldots, 2^{j'}-1 \ , \end{cases}$$

which follow from Eqs. (3.19) and the scale-evolution diagram of Fig. 5. Because of Eq. (3.18), the recursion relation of the characteristic function (3.4) for the *wavelet correlations* of the p model,

$$Z^{(j+1)}[\vec{\eta}^{(j+1)}] = \frac{1}{2}\{Z^{(j)}[(1+\alpha)\vec{\eta}_L^{(j)}]Z^{(j)}[(1-\alpha)\vec{\eta}_R^{(j)}] + Z^{(j)}[(1-\alpha)\vec{\eta}_L^{(j)}]Z^{(j)}[(1+\alpha)\vec{\eta}_R^{(j)}]\}, \tag{3.21}$$

is identical to Eq. (3.8).

The wavelet correlation densities are now given as partial derivatives of this characteristic function with respect to the η variables [compare with Eq. (3.5)]. With the transformation (3.20) we can express the derivatives with respect to $\eta^{(j+1)}$ in terms of derivatives with respect to $\eta_L^{(j)}$ and $\eta_R^{(j)}$:

$$\frac{\partial}{\partial \eta_0^{(j+1)}} = \frac{1}{2}\frac{\partial}{\partial \eta_{0;L}^{(j)}} + \frac{1}{2}\frac{\partial}{\partial \eta_{0;R}^{(j)}},$$
$$\frac{\partial}{\partial \eta_{00}^{(j+1)}} = \frac{1}{2}\frac{\partial}{\partial \eta_{0;L}^{(j)}} - \frac{1}{2}\frac{\partial}{\partial \eta_{0;R}^{(j)}}, \tag{3.22}$$
$$\frac{\partial}{\partial \eta_{j'k'}^{(j+1)}} = \begin{cases} \dfrac{\partial}{\partial \eta_{j'-1,k';L}^{(j)}} & \text{for } k' = 0, \ldots, 2^{j'-1}-1 \\ \dfrac{\partial}{\partial \eta_{j'-1,k'-2^{j'-1};R}^{(j)}} & \text{for } k' = 2^{j'-1}, \ldots, 2^{j'}-1 \ . \end{cases}$$

Equations (3.20)–(3.22) allow us to find the recursion relations for the Haar-wavelet correlation densities. In the following we will not state the various recursion relations, but only the results which follow from them.

For the first-order Haar-wavelet correlation density we obtain

$$\tilde{\rho}_0 = 1 \quad ,$$
$$\tilde{\rho}_{(j_1k_1)} = 0 \quad \text{for } 0 \le j_1 \le J-1 \ , \ 0 \le k_1 \le 2^{j_1}-1 \ . \tag{3.23}$$

That outcome is easy to understand since all bins in the p-model cascade have an average energy density equal to one and the average fluctuation between energy densities is equal to zero.

The results for the second-order Haar-wavelet correlation density are more striking:

$$\tilde{\rho}_{00} = 1 \ ,$$
$$\tilde{\rho}_{(j_1k_1),(j_1k_1)} = \alpha^2(1+\alpha^2)^{j_1} \tag{3.24}$$
$$\text{with } 0 \le j_1 \le J-1 ; 0 \le k \le 2^{j_1}-1$$
$$\tilde{\rho}_{(j_1k_1),(j_2k_2)} = 0, \quad \text{for } (j_1,k_1) \ne (j_2,k_2) \ ;$$

see Fig. 7 and consult Fig. 2(c) for the arrangement of the wavelet amplitudes within a $2^J \times 2^J$ matrix. This correlation density matrix is diagonal. In other words, the Haar-wavelet basis represents the adequate normal coordinates for the p model. All off-diagonal contributions vanish simply because the average of the product of two differences belonging to different scales is zero; as a consequence there are no second-order correlations between different scales of the p-model cascade. As the resolution j_1 increases, the diagonal contributions reflect a power law (scaling law), which is clear evidence of the self-similarity of the p-model cascade. Compared to the two-bin correlation density (3.10), the Haar-wavelet cor-

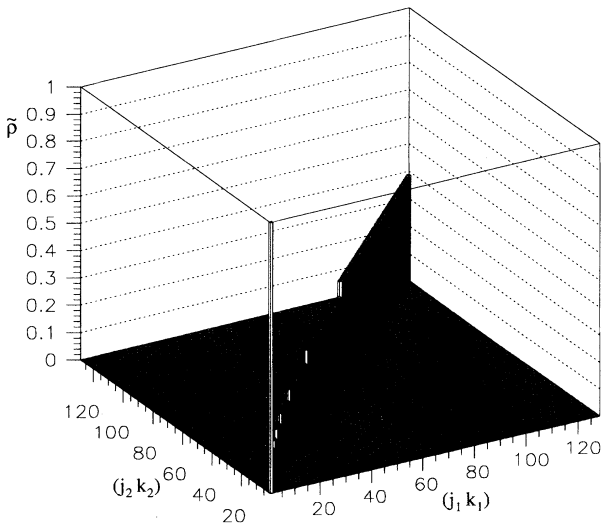

FIG. 7. Haar-wavelet transformed two-bin correlation density $\tilde{\rho}_{(j_1k_1),(j_2k_2)}$ for the p-model cascade.

relation density has a much simpler and clearer structure; compare Fig. 6 with Fig. 7.

Similar to the Haar-wavelet correlation density of second order, the one of third order also takes a simpler and sparser structure than the conventional correlation density (3.11). We will not exhibit any results here, but rather consider the corresponding Haar-wavelet cumulants.

Analogously to Eqs. (3.12)–(3.14), the Haar-wavelet cumulants subtract redundant lower-order correlations and read

$$\tilde{C}_{(j_1k_1)} = \tilde{\rho}_{(j_1k_1)} \ , \tag{3.25}$$

$$\tilde{C}_{(j_1k_1),(j_2k_2)} = \tilde{\rho}_{(j_1k_1),(j_2k_2)} - \tilde{\rho}_{(j_1k_1)}\tilde{\rho}_{(j_2k_2)} \ ,$$

$$\begin{aligned}\tilde{C}_{(j_1k_1),(j_2k_2),(j_3k_3)} &= \tilde{\rho}_{(j_1k_1),(j_2k_2),(j_3k_3)} - \tilde{\rho}_{(j_1k_1),(j_2k_2)}\tilde{\rho}_{(j_3k_3)} \\ &\quad -\tilde{\rho}_{(j_1k_1),(j_3k_3)}\tilde{\rho}_{(j_2k_2)} - \tilde{\rho}_{(j_2k_2),(j_3k_3)}\tilde{\rho}_{(j_1k_1)} \\ &\quad +2\tilde{\rho}_{(j_1k_1)}\tilde{\rho}_{(j_2k_2)}\tilde{\rho}_{(j_3k_3)} \ .\end{aligned}$$

The only difference between the second-order cumulant (3.25) and the second-order correlation density (3.24) is that

$$\tilde{C}_{00} = 0 \ ;$$

otherwise they are identical because of Eq. (3.23). This result also generalizes to the third-order Haar-wavelet cumulant in that all contributions involving the roughest scaling function now vanish. The only remaining and nonvanishing contributions to the third-order Haar-wavelet cumulant are given by

$$\tilde{C}_{(j_2k_2),(j_2k_2),(j_1k_1)} = (1+3\alpha^2)^{j_1}\left[\pm 2\alpha^4(1+\alpha^2)^{j_2-j_1-1}\right] \ , \tag{3.26}$$

with $0 \le j_1 < j_2 \le J-1$ and $(k_1+1)2^{j_2-j_1} \le k_2 \le k_1 2^{j_2-j_1} + 2^{j_2-j_1-1} - 1$ for the plus sign and $k_1 2^{j_2-j_1} + 2^{j_2-j_1-1} \le k_2 \le (k_1+1)2^{j_2-j_1} - 1$ for the minus sign. Illustratively, the restrictions on the indices indicate that the third-order Haar-wavelet cumulant is only nonvanishing if the indices (j_1,k_1) and (j_2,k_2) have the same "parenthood," where the plus (minus) sign has to be chosen if (j_2,k_2) belongs to the left (right) branch of the cascading tree starting in (j_1,k_1). We have a *double* power law, which depends on the rougher scale j_1 and the difference $j_2 - j_1$ of the two involved scales; this is exemplified in Fig. 8.

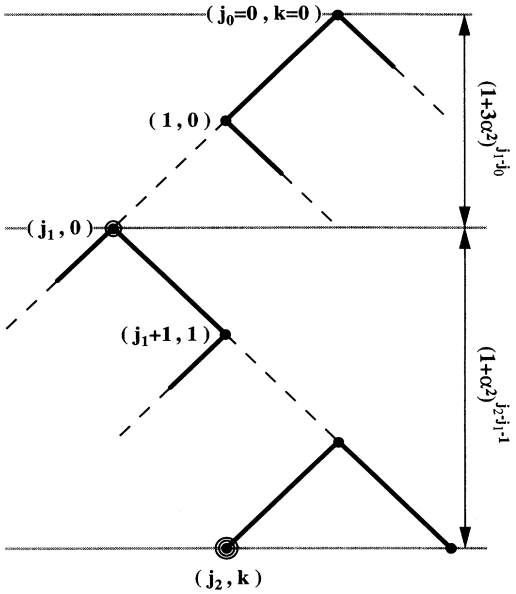

FIG. 8. Double scaling of the third-order Haar wavelet cumulant $\tilde{C}_{(j_2k_2),(j_2k_2),(j_1k_1)}$ for the p-model cascade.

D. General wavelet correlation densities

Evidently, the Haar-wavelet basis represents the true normal coordinates for the p-model density cascade, since it diagonalizes the corresponding covariance matrix (equal to the second-order correlation density matrix) completely. For more general wavelets this result will not hold exactly. However, we could hope that they might lead to a quasidiagonalization of the covariance matrix; this means that the off-diagonal contributions are strongly suppressed compared to the diagonal contributions.

It should be clear from the very beginning that the direct determination of the Haar-wavelet correlations for the p model, as presented in the preceding subsection, will no longer be feasible for more complicated wavelets. Therefore we develop a formalism that will allow us to determine the wavelet correlation densities directly from the bin correlation densities.

We start with a suitable generalization of Eqs. (2.5):

$$\begin{aligned}\epsilon(x) \longrightarrow \epsilon^{(J)}(x) &= \sum_{k=0}^{2^J-1} \epsilon_k \phi_{Jk}(x) \\ &= \epsilon_0^{(0)}\phi_{00}(x) + \sum_{j=0}^{J-1}\sum_{k=0}^{2^j-1} \tilde{\epsilon}_{jk}\psi_{jk}(x) \ ,\end{aligned} \tag{3.27}$$

where the Haar scaling function $\phi_{Jk}^H(x)$ has been replaced by an arbitrary orthogonal scaling function $\phi_{Jk}(x)$. This leads to a modified multiresolution analysis. The resulting "histograms" at the various scales are now not discontinuous step functions as in Fig. 1, but acquire the smoothness and other properties of the underlying scaling function and wavelet. For this more general multiresolution analysis it is necessary to impose a periodic continuation of $\epsilon(x)$ outside its support, which is a common practice to reduce unwanted edge effects.

Equation (3.27) can be viewed as a linear transformation of the amplitudes ϵ_k, written compactly as

$$\vec{\epsilon} = (\epsilon_0, \epsilon_1, \epsilon_2, \ldots, \epsilon_{2^J-1}) \ , \tag{3.28}$$

to the wavelet amplitudes $\tilde{\epsilon}_{jk}$

$$\begin{aligned}\vec{\tilde{\epsilon}} &= (\epsilon_0^{(0)}, \tilde{\epsilon}_{00}, \tilde{\epsilon}_{10}, \tilde{\epsilon}_{11}, \tilde{\epsilon}_{20}, \ldots, \tilde{\epsilon}_{23}, \tilde{\epsilon}_{30}, \ldots, \tilde{\epsilon}_{J-1,2^{J-1}-1}) \\ &=: (\tilde{\epsilon}_0 \ , \tilde{\epsilon}_1 \ , \tilde{\epsilon}_2 \ , \tilde{\epsilon}_3 \ , \tilde{\epsilon}_4 \ , \ldots, \tilde{\epsilon}_7 \ , \tilde{\epsilon}_8 \ , \ldots, \tilde{\epsilon}_{2^J-1}) \ ,\end{aligned} \tag{3.29}$$

so that

$$\vec{\tilde{\epsilon}} = \mathbf{W}\vec{\epsilon} \ . \tag{3.30}$$

Note that the transformation matrix $\mathbf{W}$ depends only on the coefficients c_m of Eqs. (2.8) and (2.9). More details about its structure are given in the Appendix. For the characteristic function (3.4) we derive

$$\begin{aligned}Z[\vec{\lambda}] &= \left\langle \exp\left(i\vec{\lambda}\cdot\vec{\epsilon}\right)\right\rangle = \left\langle \exp\left(i\vec{\lambda}\mathbf{W}^{-1}\cdot\mathbf{W}\vec{\epsilon}\right)\right\rangle \\ &= \left\langle \exp\left\{i\left[\left(\mathbf{W}^{-1}\right)^T\vec{\lambda}\right]\cdot\vec{\tilde{\epsilon}}\right\}\right\rangle = \left\langle \exp\left(i\vec{\eta}\cdot\vec{\tilde{\epsilon}}\right)\right\rangle \\ &= Z[\vec{\eta}] \ .\end{aligned} \tag{3.31}$$

The new set of variation parameters

$$\vec{\eta} = (\eta_0, \eta_{00}, \eta_{10}, \eta_{11}, \ldots, \eta_{J-1,2^{J-1}-1}) \tag{3.32}$$

are the wavelet transformed $\vec{\lambda}$:

$$\vec{\eta} = \left(\mathbf{W}^{-1}\right)^T\vec{\lambda} \ . \tag{3.33}$$

The wavelet correlation densities are obtained by appropriate derivatives of the characteristic function with respect to the η variables. For example, the first-order wavelet correlation density reads

$$\begin{aligned}\tilde{\rho}_{k_1} &= \frac{1}{i}\left.\frac{\partial Z[\vec{\eta}]}{\partial\eta_{k_1}}\right|_{\vec{\eta}=0} \\ &= \sum_{k_2=0}^{2^J-1}\frac{\partial\lambda_{k_2}}{\partial\eta_{k_1}}\frac{1}{i}\left.\frac{\partial Z[\vec{\lambda}]}{\partial\lambda_{k_2}}\right|_{\vec{\lambda}=0} \\ &= \sum_{k_2=0}^{2^J-1}(\mathbf{W}^T)_{k_2k_1}\rho_{k_2} = \sum_{k_2=0}^{2^J-1}(\mathbf{W})_{k_1k_2}\rho_{k_2} \ .\end{aligned} \tag{3.34}$$

For the second- and third-order wavelet correlation densities we obtain analogously

$$\tilde{\rho}_{k_1k_3} = \sum_{k_2,k_4}(\mathbf{W})_{k_1k_2}(\mathbf{W})_{k_3k_4}\rho_{k_2k_4} \ , \tag{3.35}$$

$$\tilde{\rho}_{k_1k_3k_5} = \sum_{k_2,k_4,k_6}(\mathbf{W})_{k_1k_2}(\mathbf{W})_{k_3k_4}(\mathbf{W})_{k_5k_6}\rho_{k_2k_4k_6} \ .$$

This approach is model independent and applicable for any compact wavelet. The only prerequisite is that the bin correlation densities are known, as is the case for the p model studied here [Eqs. (3.9)–(3.11)].

Figure 9 shows the result for the second-order D4-wavelet correlation density $\tilde{\rho}_{k_3k_4} = \tilde{\rho}_{(j_1k_1),(j_2k_2)}$. The dominating contributions are on the diagonal and also indicate a scaling, which, besides fluctuations, is approximately equal to the scaling occurring in the Haar-wavelet case of Fig. 7. Off-diagonal contributions arise in bands, which reflect correlations between different scales belonging to the same evolution branch of the p-model cascade tree. Although, as expected, the D4-wavelet basis does not lead to a complete diagonalization of the covariance matrix, it gives rise to a quasidiagonalization since off-diagonal contributions are strongly suppressed with respect to the diagonal contributions. This quasidiagonalization of the covariance matrix for self-similar stochastic processes seems to be a general feature of the wavelet basis.

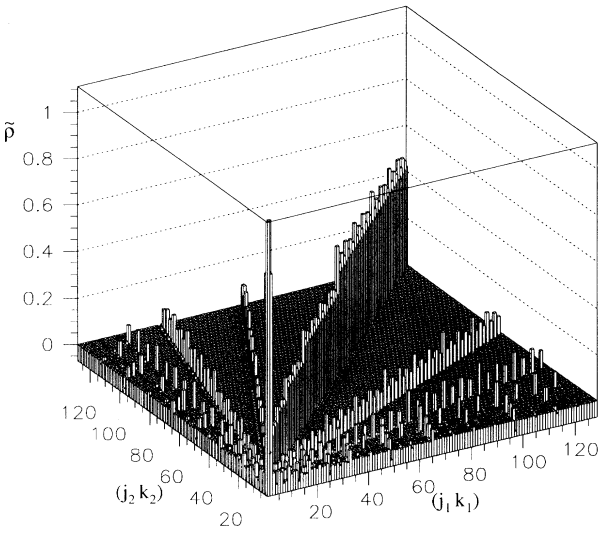

FIG. 9. D4-wavelet transformed two-bin correlation density $\tilde{\rho}_{(j_1k_1),(j_2k_2)}$ for the p-model cascade.

In the case that the bin correlation densities are not known analytically, such as for experimental data or more complicated models, the wavelet correlation densities have to be sampled from N independent events (configurations). The multiresolution decomposition (3.30) is then applied to each event and the wavelet correlation densities are obtained by

$$\begin{aligned}\tilde{\rho}_{(j_1k_1)} &= \frac{1}{N}\sum_{\mu=1}^{N}\tilde{\epsilon}_{j_1k_1} \ , \\ \tilde{\rho}_{(j_1k_1)(j_2k_2)} &= \frac{1}{N}\sum_{\mu=1}^{N}\tilde{\epsilon}_{j_1k_1}\tilde{\epsilon}_{j_2k_2} \ , \ldots \ .\end{aligned} \tag{3.36}$$

IV. WAVELET CORRELATIONS OF POINT DISTRIBUTIONS AND POISSONIAN NOISE

So far we have discussed *ordinary* moments and their wavelet transforms for *continuous* positive random variables $(\epsilon_0, \ldots, \epsilon_{2^J-1})$. In this section we extend our considerations to *discrete* random variables $(n_0, \ldots, n_{2^J-1})$ with $n_k = 0, 1, 2, \ldots$, *factorial* moment densities and their respective wavelet transforms.

For discrete counting problems the appropriate statistical framework is that of point distributions. Given an

event with $\hat{N}$ particles at positions $(\hat{x}_1, \ldots, \hat{x}_{\hat{N}})$, we define the point density (see, e.g., [12])

$$\hat{\rho}(x) = \sum_{i=1}^{\hat{N}} \delta(x - \hat{x}_i) \ , \tag{4.1}$$

which can be regarded as a histogram with infinite resolution. Factorial moment densities of qth order are obtained by event averaged products of $\hat{\rho}(x)$

$$\begin{aligned} \rho_{[q]}(x_1, \ldots, x_q) &= \left\langle \hat{\rho}_{[q]}(x_1, \ldots, x_q) \right\rangle \\ &= \left\langle \sum_{i_1 \neq \cdots \neq i_q} \delta(x_1 - \hat{x}_{i_1}) \cdots \delta(x_q - \hat{x}_{i_q}) \right\rangle \ , \end{aligned} \tag{4.2}$$

with the restriction that the same particle may not be counted more than once. Note that the corresponding ordinary moment densities ρ_q are obtained by allowing for multiple counts of the same particle, i.e., replacing the restricted sum by the free one $\sum_{i_1,\ldots,i_q}$ in Eq. (4.2).

We define factorial wavelet correlations by the multiresolution expansion of the qth factorial moment density; for simplicity, we exhibit only second-order densities:

$$\begin{aligned} \rho_{[2]}(x_1, x_2) = \sum_{j_1, j_2} \sum_{k_1, k_2} & \tilde{\rho}_{[2]}(j_1, k_1; j_2, k_2) \\ & \times \psi_{j_1 k_1}(x_1)\, \psi_{j_2 k_2}(x_2) \ , \end{aligned} \tag{4.3}$$

where the summation $\sum_{j_1 j_2}$ also includes the terms involving the scaling function ϕ_{00} at the roughest scale.

The wavelet transformed factorial densities are defined by

$$\begin{aligned} \tilde{\rho}_{[2]}(j_1, k_1; j_2, k_2) &= 2^{j_1 + j_2} \left\langle \int \hat{\rho}_{[2]}(x_1, x_2)\, \psi_{j_1 k_1}(x_1)\, \psi_{j_2 k_2}(x_2)\, dx_1 dx_2 \right\rangle \\ &= 2^{j_1 + j_2} \left\langle \sum_{i_1 \neq i_2} \psi_{j_1 k_1}(\hat{x}_{i_1})\, \psi_{j_2 k_2}(\hat{x}_{i_2}) \right\rangle \ , \end{aligned} \tag{4.4}$$

using the δ–function representation (4.2). Equation (4.4) and its trivial extension to higher orders provide an easily computable sampling prescription for factorial wavelet correlations of point distributions. All one needs to know is the functional form of $\psi(x)$.

In particle physics and particularly in intermittency studies, factorial moments are favored over ordinary ones based on the argument that the former unfold "statistical" fluctuations from "dynamical" ones. This picture, promoted in the original work of Białas and Peschanski [1], is based on the Poisson transform. More specifically, in a Poisson transformed histogram at resolution J each continuous random density ϵ_k is replaced by a discrete random number n_k of particles, where each n_k is tossed, independently from any other bin, according to a Poissonian

$$p_{n_k}(\epsilon_k) = \exp(-\bar{n}\epsilon_k) \frac{(\bar{n}\epsilon_k)^{n_k}}{n_k!} \ . \tag{4.5}$$

The average number of particles per bin $\bar{n} = \sum_k \langle n_k \rangle / 2^J$ is a free parameter. In a subsequent step the n_k particles are uniformly distributed over the kth bin; see Fig. 4.

Białas and Peschanski refer to correlations at the level of the ϵ_k as "dynamical fluctuations" and those at the level of the Poisson transformed n_k as "dynamical fluctuations with statistical (or Poissonian) noise." Adopting this terminology, the mentioned unfolding property means that the ordinary moments of the ϵ_k are proportional to the factorial moments of the n_k [1]:

$$\begin{aligned} \rho^{\text{noise}}_{[2]}(k_1, k_2) &= \langle n_{k_1} n_{k_2} \rangle - \delta_{k_1 k_2} \langle n_{k_1} \rangle \\ &= \bar{n}^2 \langle \epsilon_{k_1} \epsilon_{k_2} \rangle = \bar{n}^2 \rho^{\text{dyn}}_{k_1, k_2} \ . \end{aligned} \tag{4.6}$$

Taking the wavelet transforms of both sides we conclude that a similar relation holds for wavelet correlations:

$$\tilde{\rho}^{\text{noise}}_{[2]}(j_1, k_1; j_2, k_2) = \bar{n}^2 \tilde{\rho}^{\text{dyn}}_{(j_1 k_1), (j_2 k_2)} \ . \tag{4.7}$$

Of course, this argument is extendable to all higher orders. Hence the unfolding property of standard factorial moments also pertains to suitably defined factorial wavelet moments (4.4).

At this point we mention that appropriate wavelet factorial cumulants can be defined by a straightforward extension of (4.4) to linear combinations of products of densities $\rho_{[q]}$. Note, however, that the direct sampling of both the standard and wavelet transformed cumulants requires the use of event-mixing techniques [3].

V. CONCLUSIONS AND OUTLOOK

The main goal of this study is to explore the wavelet transform applied to correlation studies. Orthogonal wavelets define a *multiresolution representation* of a (random) signal, which dissects the latter into contributions from different scales. We expect that data arising from hierarchically organized random processes exhibit a uniquely simple correlation structure once they are represented in an appropriate wavelet basis.

These expectations are supported by studies of fractional Brownian motion [9] as well as by the present analysis of a simple cascade model. In both scenarios the correlations between contributions from different scales nearly decouple, or in other words, the covariance matrix of the wavelet transformed signal takes a quasidiagonal form. In the case of the self-similar p model we have shown that the simple Haar-wavelet diagonalizes the covariance matrix even *exactly* and, moreover, the diagonal contributions belonging to different scales exhibit a scaling law. For the third-order Haar-wavelet cumulants we have found a double scaling in the sense that con-

tributions with a common parenthood depend on their absolute as well as their relative scale with respect to the common ancestor. More general wavelets, such as, for example, the Daubechies D4 wavelets, are not ideal normal coordinates for the p model and lead only to a quasidiagonalization of the covariance matrix. The power-law scaling along the diagonal is still recovered, but now minor off-diagonal contributions arise in band structures, which reflect small correlations between D4 fluctuations at different scales.

Besides the study of correlations in continuous random functions it is also important to discuss correlations of point distributions. The latter are usually studied in terms of factorial moments or product densities. We defined appropriate factorial wavelet correlation functions which share all the nice properties of standard factorials. We recalled that the normalized factorials for the p model with Poissonian noise are identical to the underlying p-model density correlations; in other words, noise has been unfolded. Of course this correspondence is *preserved* by the wavelet transform.

The results of this paper are no more than a preliminary study; there is still a long way to go. For multiparticle physics the above observations let us hope that the successive "local smoothing" and "differentiation" operations of an appropriate multiresolution decomposition might facilitate comparisons of experimental cluster-correlation studies at the hadron level with theoretical calculations of parton shower models. We further believe that wavelet correlations serve as a useful tool to study the self-similarity aspect of QCD parton cascades, which occur in e^+e^- and hadron-hadron collisions. Of course, these hopes and expectations remain to be verified by further analyses.

Also outside multiparticle physics wavelet correlations might prove to be useful. Recently we became aware of more elaborate studies about intermittency in fully developed turbulence [13]. There is evidence that turbulent cascades show some interscale correlations. In this respect, wavelet correlations offer an ideal tool to gain further insight into these phenomena.

ACKNOWLEDGMENTS

We would like to thank B. Buschbeck for helpful discussions and support. One of us (M.G.) would like to thank Alexander von Humboldt Stiftung and the Deutsche Forschungsgemeinschaft for financial support. This work was supported by the U.S. Department of Energy, Grant No. DE-FG02-88ER40456, and by the Austrian Fonds zur Förderung der Wissenschaftlichen Forschung, Project No. P8259–TEC.

APPENDIX: THE WAVELET TRANSFORMATION MATRIX W

We restrict this consideration to the compact and orthogonal Daubechies D4 wavelet only; the generalization to other wavelets is straightforward.

According to the general multiresolution analysis defined by dilation equations (2.8) and (2.9) we can write

$$\begin{pmatrix} \phi_{J-1,0} \\ \phi_{J-1,1} \\ \vdots \\ \phi_{J-1,2^{J-1}-2} \\ \phi_{J-1,2^{J-1}-1} \\ \psi_{J-1,0} \\ \psi_{J-1,1} \\ \vdots \\ \psi_{J-1,2^{J-1}-2} \\ \psi_{J-1,2^{J-1}-1} \end{pmatrix} = \underbrace{\begin{pmatrix} c_0 & c_1 & c_2 & c_3 & 0 & 0 & \cdots & 0 & 0 & 0 & 0 \\ 0 & 0 & c_0 & c_1 & c_2 & c_3 & \cdots & 0 & 0 & 0 & 0 \\ & & & \ddots & & & \ddots & & & & \\ 0 & 0 & 0 & 0 & & \cdots & & c_0 & c_1 & c_2 & c_3 \\ c_2 & c_3 & 0 & 0 & & \cdots & & 0 & 0 & c_0 & c_1 \\ c_1 & -c_0 & 0 & 0 & & \cdots & & 0 & 0 & c_3 & -c_2 \\ c_3 & -c_2 & c_1 & -c_0 & & \cdots & & 0 & 0 & 0 & 0 \\ & & & & \ddots & & & \ddots & & & \\ 0 & 0 & 0 & 0 & \cdots & c_3 & -c_2 & c_1 & -c_0 & 0 & 0 \\ 0 & 0 & 0 & 0 & \cdots & 0 & 0 & c_3 & -c_2 & c_1 & -c_0 \end{pmatrix}}_{\mathbf{A}^{(J)}} \begin{pmatrix} \phi_{J,0} \\ \phi_{J,1} \\ \vdots \\ \phi_{J,2^{J-1}-2} \\ \phi_{J,2^{J-1}-1} \\ \phi_{J,2^{J-1}} \\ \phi_{J,2^{J-1}+1} \\ \vdots \\ \phi_{J,2^J-2} \\ \phi_{J,2^J-1} \end{pmatrix}, \tag{A1}$$

where $\mathbf{A}^{(J)}$ is a $2^J \times 2^J$ orthogonal matrix. In the next step the scaling functions $\phi_{J-1,k}$ are rewritten in terms of the scaling functions $\phi_{J-2,k}$ and the wavelets $\psi_{J-2,k}$, whereas the wavelets $\psi_{J-1,k}$ are kept; this procedure is repeated over and over again until the scale $j = 1$ is reached. With the abbreviation

$$\begin{aligned} \vec{\psi} &= (\phi_{10}, \phi_{11}, \psi_{10}, \psi_{11}, \psi_{20}, \ldots, \psi_{23}, \psi_{30}, \ldots, \psi_{J-1,2^{J-1}-1}), \\ \vec{\phi} &= (\phi_{J0}, \phi_{J1}, \phi_{J2}, \phi_{J3}, \phi_{J4}, \ldots, \phi_{J7}, \phi_{J8}, \ldots, \phi_{J,2^J-1}), \end{aligned} \tag{A2}$$

we get, for the overall transformation matrix,

$$\begin{aligned} \vec{\psi} &= \tilde{\mathbf{A}}^{(2)} \cdot \tilde{\mathbf{A}}^{(3)} \ldots \tilde{\mathbf{A}}^{(J-1)} \cdot \mathbf{A}^{(J)} \vec{\phi} \\ &=: (\mathbf{W}^T)^{-1} \vec{\phi}, \end{aligned} \tag{A3}$$

where the $2^J \times 2^J$ matrix

$$\tilde{\mathbf{A}}^{(j)} = \begin{pmatrix} \mathbf{A}^{(j)} & 0 \\ 0 & \mathbf{1} \end{pmatrix} \tag{A4}$$

is constructed from the $2^j \times 2^j$ matrix $\mathbf{A}^{(j)}$, which has a structure analogous to that of $\mathbf{A}^{(J)}$.

Equation (A3) defines the wavelet transformation matrix $\mathbf{W}$ introduced in Eq. (3.30). The wavelet expansion (3.27) can then be written as

$$\vec{\epsilon} \cdot \vec{\phi} = (\mathbf{W}^{-1}\vec{\tilde{\epsilon}}) \cdot (\mathbf{W}^T\vec{\psi}) = \vec{\tilde{\epsilon}}(\mathbf{W}^{-1})^T \cdot \mathbf{W}^T\vec{\psi} = \vec{\tilde{\epsilon}} \cdot \vec{\psi} \ . \tag{A5}$$

Note that the matrix $(\mathbf{W}^{-1})^T$ differs from $\mathbf{W}$ by normalization factors 2^{-j} in appropriate places.

[1] A. Białas and R. Peschanski, Nucl. Phys. B **273**, 703 (1986); **308**, 857 (1988).

[2] See, for example, C.B. Chiu and R.C. Hwa, Phys. Rev. D **43**, 100 (1991); S. Hegyi, Phys. Lett. B **309**, 443 (1993).

[3] H.C. Eggers, P. Lipa, P. Carruthers, and B. Buschbeck, Phys. Rev. D **48**, 2040 (1993).

[4] W. Ochs and J. Wosiek, Phys. Lett. B **289**, 159 (1992); **304**, 144 (1993); Ph. Brax, J.-L. Meunier, and R. Peschanski, Z. Phys. C **62**, 649 (1994); G. Gustafsson and A. Nilsson, *ibid.* **52**, 533 (1991).

[5] S. Mallat, IEEE Trans. Pattern Anal. Machine Intell. **11**, 674 (1989).

[6] I. Daubechies, Commun. Pure Appl. Math. **41**, 909 (1988); *Ten Lectures on Wavelets* (SIAM, Philadelphia, 1992).

[7] Y. Meyer, *Wavelets and Operators* (Cambridge University Press, New York, 1992); *Wavelets: Algorithms and Applications* (SIAM, Philadelphia, 1993).

[8] M.B. Ruskai *et al.*, *Wavelets and Their Application* (Jones and Bartlett, Boston, 1992).

[9] J. Ramanathan and O. Zeitouni, IEEE Trans. Inf. Theory **37**, 1156 (1991); A.H. Tewfik and M. Kim, *ibid.* **38**, 904 (1992); P. Flandrin, *ibid.* **38**, 910 (1992).

[10] C. Meneveau and K.R. Sreenivasan, Phys. Rev. Lett. **59**, 1424 (1987).

[11] P. Lipa and B. Buschbeck, Phys. Lett. B **223**, 465 (1989).

[12] P. Carruthers, H.C. Eggers, and I. Sarcevic, Phys. Lett. B **245**, 258 (1991); P. Carruthers, Phys. Rev. A **43**, 2632 (1991).

[13] K.R. Sreenivasan and G. Stolovitzky, J. Stat. Mech. (to be published).